The Realization of Extreme Tornadic Storm Events under Future Anthropogenic Climate Change

ROBERT J. TRAPP

Department of Atmospheric Sciences, University of Illinois at Urbana–Champaign, Urbana, Illinois

KIMBERLY A. HOOGEWIND

Department of Earth, Atmospheric, and Planetary Sciences, Purdue University, West Lafayette, Indiana

(Manuscript received 31 August 2015, in final form 4 April 2016)

ABSTRACT

This research seeks to answer the basic question of how current-day extreme tornadic storm events might be realized under future anthropogenic climate change. The pseudo global warming (PGW) methodology was adapted for this purpose. Three contributions to the CMIP5 archive were used to obtain the mean 3D atmospheric state simulated during May 1990–99 and May 2090–99. The climate change differences (or Δs) in temperature, relative humidity, pressure, and winds were added to NWP analyses of three high-end tornadic storm events, and this modified atmospheric state was then used for initial and boundary conditions for real-data WRF Model simulations of the events at high resolution. Comparison of an ensemble of these simulations with control simulations (CTRL) facilitated assessment of PGW effects.

In contrast to the robust development of supercellular convection in each CTRL, the combined effects of increased convective inhibition (CIN) and decreased parcel lifting under PGW led to a failure of convection initiation in many of the experiments. Those experiments that had sufficient matching between the CIN and lifting tended to generate stronger convective updrafts than CTRL, although not in proportion to the projected higher levels of convective available potential energy (CAPE) under PGW. In addition, the experiments with enhanced updrafts also tended to have enhanced vertical rotation. In fact, such supercellular convection was even found in simulations that were driven with PGW-reduced environmental wind shear. Notably, the PGW modifications did not induce a change in the convective morphology in any of the PGW experiments with significant convective storminess.

1. Introduction

A persistent uncertainty in climate change assessments to date regards how the frequency and intensity of local, high-impact convective storms might be affected by the global radiative forcing due to anthropogenically enhanced greenhouse gas concentrations. Much of this uncertainty can be attributed to the fact that convective storms as well as their attendant hazards have spatial scales that fall well below the effective resolution of typical global and even regional climate models.

As first demonstrated by Trapp et al. (2007), Del Genio et al. (2007), and Marsh et al. (2007), this model-resolution issue can be partly overcome through the use of environmental proxies—that is, convective-storm occurrences represented through quantifications of the larger-scale distributions of temperature, humidity, and wind that comprise the storm's "environment." Following Brooks et al. (2003b), exceedances of a thresholded product of convective available potential energy (CAPE) and vertical wind shear over a surface-to-6-km layer constitute one widely used means of representing the frequency of severe thunderstorms, which by definition generate tornadoes, hail, and/or damaging straight-line winds. Save for some temporal and geographical details, a common finding among the proxy-based studies is an increase in the frequency of severe-thunderstorm environments under anthropogenic climate change.

Beyond the mismatch between the occurrence of an environment and the actual occurrence of severe thunderstorm, a weakness of this environmental proxy approach is that it does not unambiguously discriminate

Corresponding author address: Robert J. Trapp, Department of Atmospheric Sciences, UIUC, 105 S. Gregory St., Urbana, IL 61801. E-mail: jtrapp@illinois.edu

DOI: 10.1175/JCLI-D-15-0623.1

between the hazards that define severe thunderstorms. This owes to the fact that there is overlap between the respective environments that can support tornadoes, hail, and straight-line winds and implicitly because of the overlap between the types of organizational modes or convective-storm morphologies supported in such environments (e.g., Thompson et al. 2012). For example, geographical coexistence of supercell thunderstorms, which are responsible for most (though not all) devastating tornadoes (e.g., Trapp et al. 2005; Duda and Gallus 2010), and a squall line, which predominately generates swaths of straight-line wind damage, is not uncommon.

It is partly for this reason that convective-weather–climate applications of high-resolution regional models were introduced by Trapp et al. (2011) and then further implemented by Robinson et al. (2013) and Gensini and Mote (2015). In the latter study, the regional model was used as a means to dynamically downscale global climate model (GCM) simulations of late-twenty-first-century climate. Horizontal grid lengths on the order of several kilometers were employed in all of these model implementations so that convective processes could be treated without a parameterization. Such convection-permitting dynamical downscaling is therefore well suited for investigations of climate statistics of severe thunderstorms and attendant weather hazards. Trapp et al. (2011) established, for example, that the seasonality and geographical distributions of current-climate severe thunderstorms could be well represented by the downscaling approach (see also Robinson et al. 2013; Gensini and Mote 2014). Gensini and Mote (2015) then found a significant increase in the frequency of downscaled severe-thunderstorm occurrences during 2080–90 relative to 1980–90, albeit primarily in the month of March and within the Mississippi, Tennessee, and Ohio River valleys.

The statistics generated through downscaling have tended to focus on the geospatial coverage and frequency of the thunderstorms during the interval of interest. This implies a lack of concern about the fidelity of known historical events that might have happened during the interval and therefore about the projection of these events in the future. Indeed, there is no expectation that the GCM simulations of the current climate will yield identical weather patterns at specific dates to those observed and consequently no expectation that the downscaled simulations will result in identical thunderstorms to those observed.

This leads us to our current work on historical extreme events: herein we ask whether a set of high-end tornadic storms would be more intense, and/or realized as a different morphology, given late-twenty-first-century conditions induced by anthropogenic climate change. A more specific question is as follows: Will the significantly tornadic supercells from the current and past climates become the nontornadic squall lines in the future climate? These questions arise, but are generally unanswerable, from using thunderstorm environmental proxies and even traditional dynamical downscaling. Thus, we employ the pseudo global warming (PGW) methodology introduced by Schär et al. (1996) and Frei et al. (1998) and recently used by Rasmussen et al. (2011) and Lackmann (2013, 2015). In brief, the PGW methodology involves the simulation of some event using its 3D meteorological forcing but modified by a climate change difference (or Δ). In terms of temperature, such a modification is expressed symbolically as follows:

$$T(x, y, z, t) = T(x, y, z, t) + \Delta T, \tag{1}$$

where $T(x, y, z, t)$ represents the 3D, time-dependent forcing, and the climate change difference in temperature is

$$\Delta T = \overline{T(x, y, z)}_{\text{future}} - \overline{T(x, y, z)}_{\text{past}}, \tag{2}$$

as computed over some past and future time intervals.

The full PGW methodology is described in section 2, and the results of its application are given in section 3. The discussion in section 4 constitutes an attempt to use our results to interpret the results from prior studies using environmental proxies. Finally, conclusions are provided in section 5, which include a note about our future applications of the PGW methodology.

2. Methodology

a. *Three extreme tornadic storm events*

Although there are a number of possible ways for us to have designed our methodology, our choice was to select statistically and physically extreme events for PGW investigation. Such events have the highest societal and economic impact and would arguably be more impactful if the event intensity increased. Toward this end, three high-end tornado events were chosen: the enhanced Fujita (EF) rating of 5 (EF5) tornado of 4 May 2007 in Greensburg, Kansas; the EF5 tornado of 10 May 2010 in Norman, Oklahoma; and the EF4 tornado of 19 May 2013 in Shawnee, Oklahoma (hereinafter, these events will be referred to as 0504, 0510, and 0519, respectively). Tornadoes with EF ratings of 4 or 5 constitute about 1% of all tornadoes (e.g., Brooks and Doswell 2001), with an average of one EF5 tornado occurring annually in the United States.

The respective tornadoes all developed within supercell thunderstorms that initiated in the afternoon or early evening hours and thereafter rapidly intensified. As

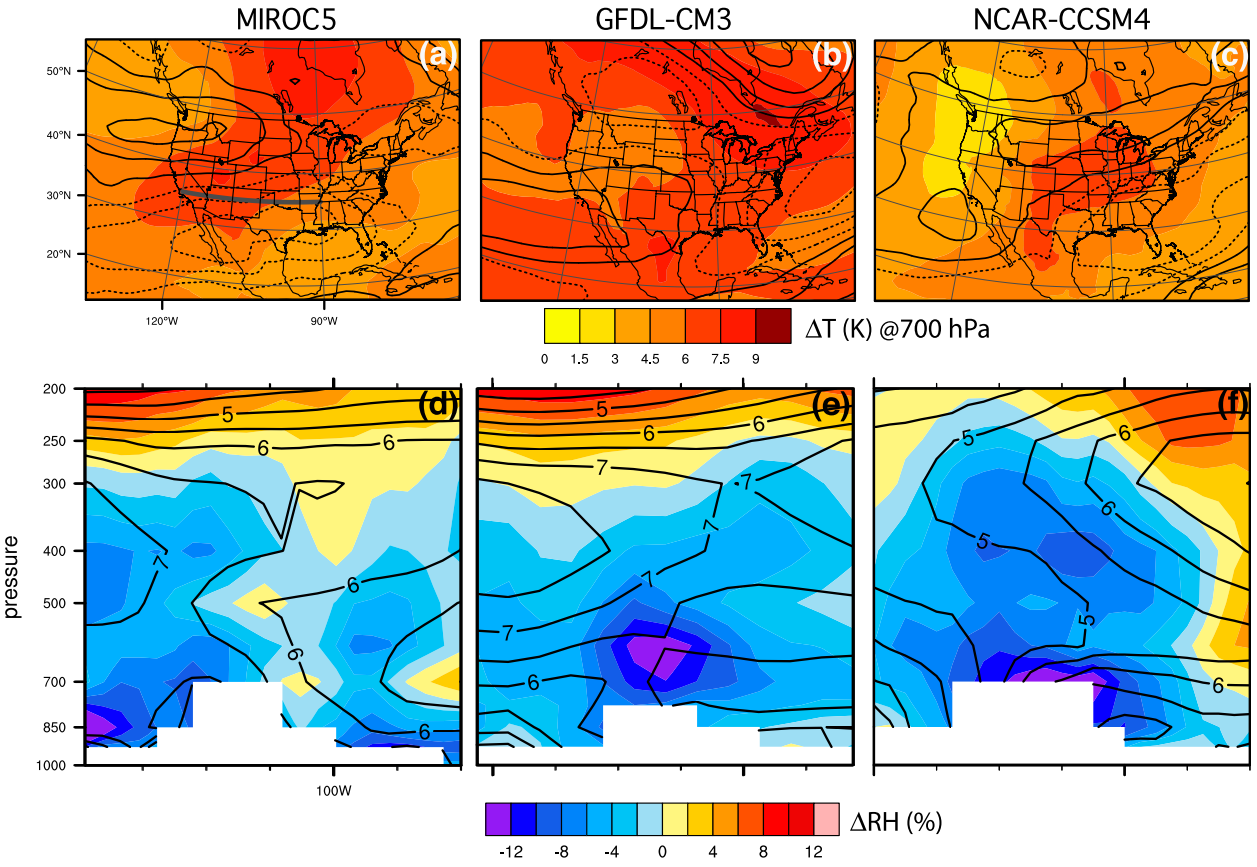

FIG. 1. Climate change Δs, or differences in the mean 3D atmospheric state between May 2090–99 and May 1990–99, from MIROC5, GFDL CM3, and CCSM4, respectively, as illustrated by (a)–(c) 500-hPa zonal wind (contours; contour interval of 1.5 m s^{-1}, with dashed lines indicating negative values) and 700-hPa temperature (color fill; K) as well as (d)–(f) relative humidity (color fill; %) and temperature (contours; contour interval of 0.5 K) in a vertical cross section. The cross section is at 35°N and extends from 120° to 90°W, as indicated by the thick gray line in (a).

discussed in more detail in section 3, the environmental conditions that supported such supercellular organization were within the established range associated with historical tornadic supercells (e.g., Grams et al. 2012). Such environmental conditions and the attendant storms are climatologically favored throughout Oklahoma and Kansas during the month of May (Brooks et al. 2003a). Thus, in a sense, the introduction of PGW should reveal how a ''typical'' extreme tornadic storm event might be realized under projected climatic conditions of the late twenty-first century.

b. PGW experiments

1) CMIP5 AND GENERATION OF CLIMATE CHANGE DIFFERENCES

Coupled atmosphere–ocean GCM simulations contributed to phase 5 of the Coupled Model Intercomparison Project (CMIP5) archive were used for the PGW experiments. The following three GCMs were drawn from the 10 analyzed by Diffenbaugh et al. (2013): MIROC5 (MI), GFDL CM3 (GF), and NCAR CCSM4 (NC). These three models showed a range of agreement with reanalysis in their portrayal of mean CAPE [and number of days with severe-thunderstorm environments (NDSEV); see Trapp et al. 2007] over March–May (MAM) 1970–99 within the southern Great Plains (SGP) region of the United States (see Fig. S9 in Diffenbaugh et al. 2013) and also showed a range of mean thunderstorm-environment frequency over the late twenty-first century. Accordingly, these three GCMs provide variability across the climate change Δs (see Fig. 1).

Following Lackmann (2013, 2015), we took the mean 3D atmospheric (temperature T, relative humidity RH, pressure p, zonal wind u, and meridional wind v) and soil (moisture and temperature) states projected during May 2090–99 and subtracted from them the states projected during May 1990–99 [e.g., Eq. (2)]; the future projection assumes a greenhouse gas scenario given by representative concentration pathway 8.5 (RCP8.5). Such climate

change Δs were generated for each GCM and then used in separate simulations of the tornadic events; this ensemble approach corresponds to that of Lackmann (2015) but differs from that of Lackmann (2013), who computed an average Δ across GCMs.

To provide a sense of these climate change Δs, we show in Fig. 1 the ΔT at 700 hPa, which consistently reveals future warming across the three models, but with variations in the geographical details. The Δu at 500 hPa has less intramodel consistency, with future decreases (increases) in the zonal wind across the SGP domain of interest indicated by MIROC5 and CCSM4 (GFDL CM3). One of our objectives is to determine whether these Δs constitute sufficient differences in forcing such that the resultant convective morphology and intensity under these various PGW conditions are significantly different than those under the present-day conditions.

2) Regional model configuration and experimentation

We used version 3.6.1 of the advanced research core of the Weather Research and Forecasting (WRF) Model (Skamarock et al. 2008) for the high-resolution regional modeling. The WRF Model was integrated over an 18-h period beginning 1200 UTC on 5 May 2007, 10 May 2010, and 19 May 2013. This early-day initialization allowed multiple hours for the generation of a mesoscale energy spectrum prior to the mid- or late-day initiation of deep convective clouds (Skamarock 2004).

The initial and boundary conditions for the WRF integrations were provided by the 6-hourly analysis product generated as part of the National Centers for Environmental Prediction (NCEP) North American Mesoscale Forecast System (NAM). Relative to other sources of initial and boundary conditions we tested, the NAM analyses (NAM-ANL) yielded the most favorable regional model control simulations, particularly in terms of the geospatial occurrence, timing, convective morphology, and general evolution of the three tornadic events.

The computational domain, which includes nested subdomains, is shown in Fig. 2. Domains denoted as d01 and d02 had horizontal grid lengths of 3 and 1 km, respectively. Two-way interactive feedbacks were afforded between d01 and d02. Both domains had 70 vertical levels, defined such that there were 13 levels within the lowest 2 km above ground level. We note here that output from d01 (3-km grid lengths) was used mostly for environmental quantifications, while output from d02 (1-km grid lengths) was used for storm-scale quantifications, but that both quantifications were conducted over the domain defined as d03, which encloses the primary tornadic storm area over the storm's key period of evolution.

As justified by the use of computational grids with horizontal lengths ≤3 km, convective processes were treated without a parameterization on all domains. Processes that were parameterized include long- and shortwave radiation (the new Goddard schemes, with calculations at 1-min intervals; Chou and Suarez 1999), cloud and precipitation microphysics (Morrison double-moment scheme; Morrison et al. 2009), turbulent eddy mixing and diffusion (horizontal Smagorinsky first-order closure scheme), planetary boundary layer (PBL) mixing (Mellor–Yamada–Janjić scheme; Janjić 1994), and land surface (Noah land surface model; Chen and Dudhia 2001). Given integration lengths of only 18 hours (and of simulated-storm evolutions lasting only a few hours), we did not vary the trace gas concentrations within the radiation parameterizations.

These particular model-physics choices were guided by high-resolution WRF simulations conducted by Van Leer (2013) as well as by our own experimentation with other parameterization schemes. As with our choice of the NAM-ANL for the initial and boundary conditions, this model-physics set yielded a favorable (qualitative) comparison to the observations in terms of the geospatial occurrence, timing, convective morphology, and general evolution of the three tornadic events. Figure 2 demonstrates that the control simulation (CTRL) of each tornadic event produced a supercell thunderstorm within an appropriate geographical domain and time.

In the PGW experiments, the 3D Δs in atmospheric temperature, humidity, pressure, winds, soil temperature, and soil moisture were added to the corresponding NAM-ANL variables [e.g., Eq. (1)]. This step was facilitated by a bilinear interpolation of the Δs to the NAM grid (which has 12-km horizontal grid lengths and 60 vertical levels) and was followed by calculations of specific humidity and geopotential height during the regional model preprocessing, using the PGW-modified variables. The nine primary PGW experiments thus consist of three simulations per tornadic event using the full climate change Δs from MIROC5, GFDL CM3, and CCSM4. There were 36 additional PGW experiments conducted as follows: three simulations per event using only the wind (u, v) Δs from MIROC5, GFDL CM3, and CCSM4; three simulations per event using only the thermodynamic (T, RH, and p) Δs from MIROC5, GFDL CM3, and CCSM4; three simulations per event using only the soil moisture and temperature Δs from MIROC5, GFDL CM3, and CCSM4; and three simulations per event using the full climate change Δs from MIROC5, GFDL CM3, and CCSM4 but with a constant-RH assumption (essentially, with $\Delta RH = 0$). Thus, excluding the three CTRL experiments, we have a 45-member ensemble to facilitate assessment of PGW effects.

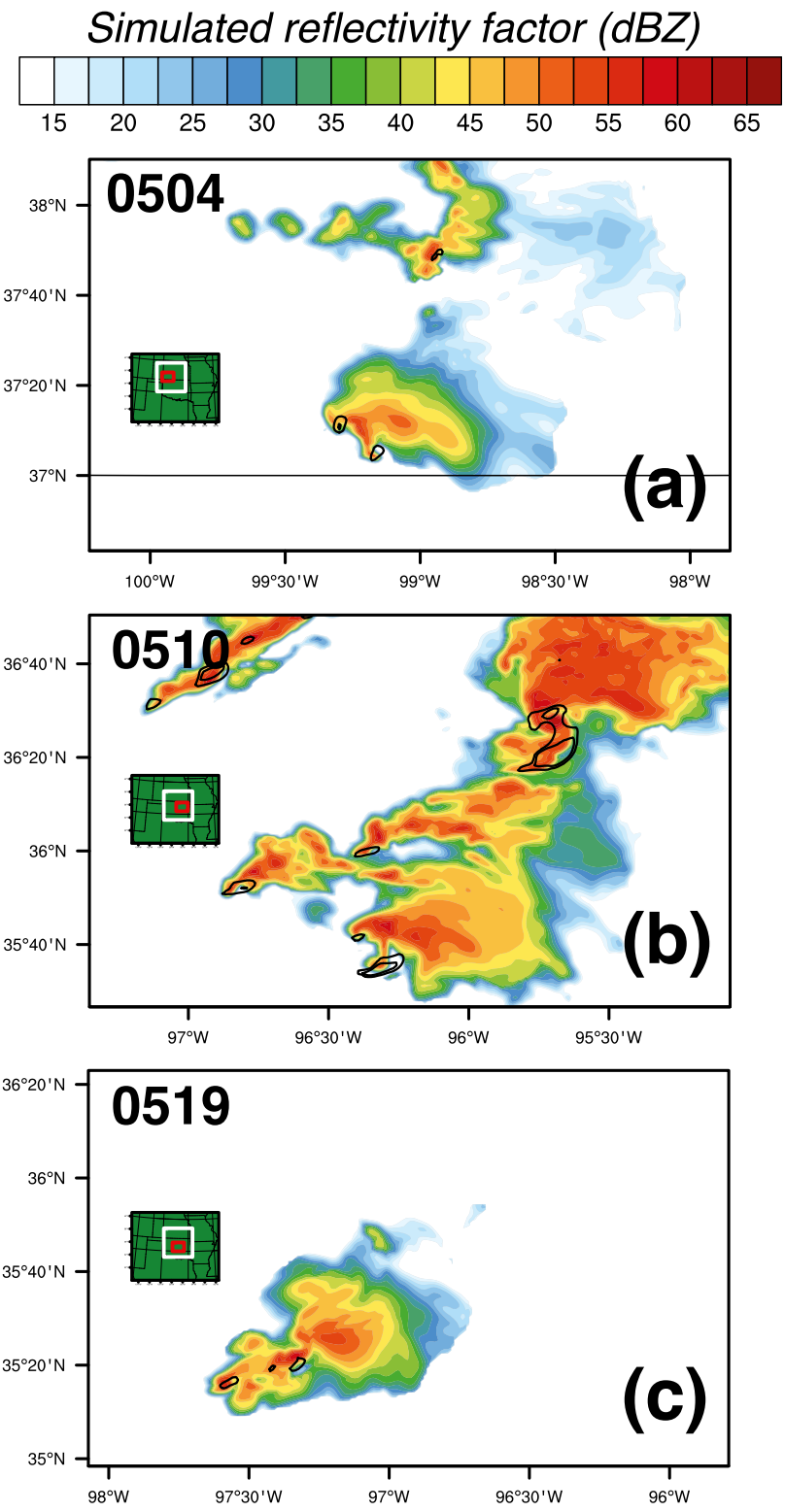

FIG. 2. Simulated reflectivity factor (color fill; dBZ) for the CTRL simulations, presented at approximately 1000 m AGL, over the area described by d03: (a) 4 May 2007 at 0225 UTC, (b) 10 May 2010 at 0100 UTC, and (c) 19 May 2013 at 2205 UTC. Contours are of updraft helicity (outer and inner contours are 450 and 900 $m^2 s^2$, respectively). The insets in each panel show the geographical areas described by domains d01 (black outline), d02 (white outline), and d03 (red outline).

3. Results

Time series plots of simulated reflectivity factor (SRF) exceeding 40 dBZ over d03 summarize the convective evolutions across the nine primary PGW experiments (Fig. 3) and in particular show that convective storms failed to initiate within d03 in four of the nine experiments (0504MI, 0504GF, 0504NC, and 0519NC) and did not fully develop in another experiment (0519MI). The lack of convection initiation is in fact a manifestation of one of the key uncertainties about deep convective storms in future climates (e.g., Trapp et al. 2007, 2009). The uncertainty is twofold: (i) whether nonuniform warming over the depth of the troposphere, and/or a drier boundary layer (e.g., see Fig. 1), will lead to increased convective inhibition (CIN) that literally is more inhibitive of parcel lifting to free convection and (ii) whether the decreased pole-to-equator temperature gradient and associated baroclinity will lead to synoptic-scale (and mesoscale) weather systems that are less capable of forcing vertical motions (w) of sufficient strength and depth to lift parcels to free convection.

Figure 4 confirms for the 0504 case that CIN is larger[1] in the PGW experiments over the domain of CTRL storm development (d03) (see Fig. 2a). As shown in Table 1, however, domain-averaged (over d03) environmental CIN ($\mathrm{CIN_{avg}}$) does not unambiguously discriminate all experiments with storm initiation from those without storm initiation; this point is illustrated well by the 0510 case, wherein a slight difference in the evolution of a warm front over d03 resulted in an overall higher $\mathrm{CIN_{avg}}$ in CTRL (at 0000 UTC; see Table 1), even though the tendency was for more widespread CIN in the PGW experiments. Indeed, the 0510 PGW experiments exhibited relatively more gridpoint occurrences of CIN $\geq 50\,\mathrm{J\,kg^{-1}}$ ($\sum$CIN), which can be considered a loose threshold for the likelihood of storm initiation. Unfortunately, $\sum$CIN is also not exclusively lower (higher) in initiating (noninitiating) experiments, and thus like $\mathrm{CIN_{avg}}$, is not a perfect predictor of storm initiation (or the lack thereof) (Table 1). Both of these quantifications imply that high CIN (and weak lifting) are not necessarily more widespread in experiments wherein convective storms failed to initiate. It is important to note, however, that storm initiation is still possible in a high-CIN environment, provided that the parcel lifting is comparably strong. This is verified by a coevaluation of CIN and w ($\sum w|$CIN), specifically, by

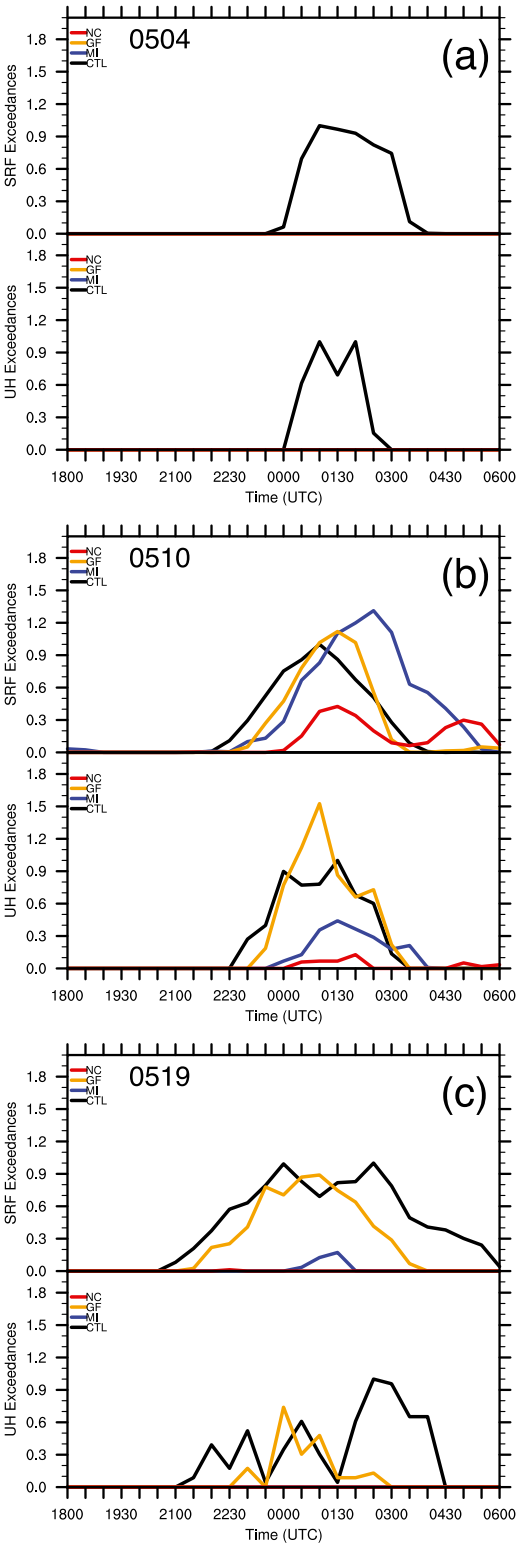

FIG. 3. Time series of gridpoint exceedances of SRF over 40 dBZ and updraft helicity over 150 $\mathrm{m^2\,s^{-2}}$ for the (a) 0504, (b) 0510, and (c) 0519 event simulations. The respective exceedances are normalized by the maximum in CTRL of each event. Evaluation is over the area described by d03 but uses d01 model fields (3-km grid spacing). The abscissa shows time in UTC. Shown are the CTRL, MI, GF, and NC experiments.

[1] The magnitude of CIN is considered here, with the convention that large CIN refers to a large amount of integrated negative buoyancy.

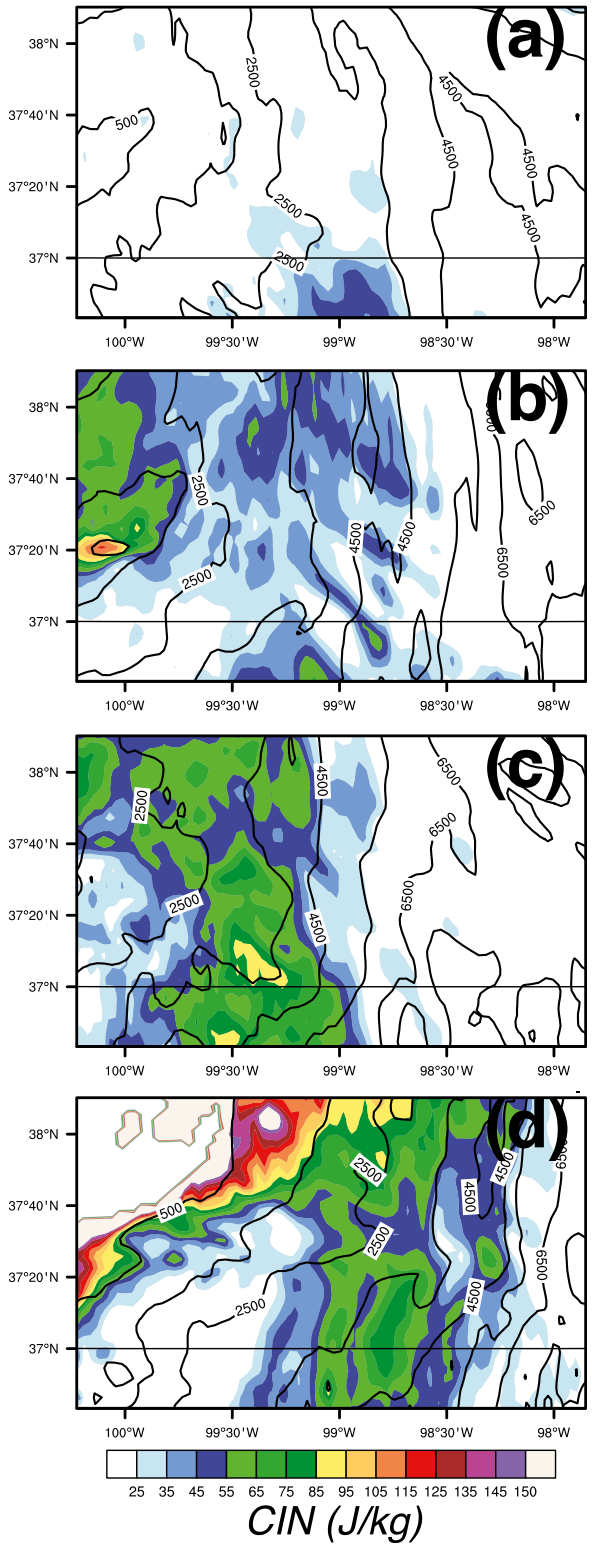

FIG. 4. Analysis of CIN (color fill; J kg^{-1}) and CAPE (contours; J kg^{-1}) over d03 and at 2300 UTC for the 0504 event simulations: (a) CTRL, (b) MI, (c) GF, and (d) NC experiments.

counts of d03 grid points where CIN ≥ 50 J kg^{-1} and $w \geq 2.5$ m s^{-1}. Table 1 and Fig. 3 clearly indicate that the experiments in which relatively large CIN was locally well matched with relatively strong parcel lifting subsequently resulted in storm initiation.

In each of the tornadic events simulated here, the baseline CIN was relatively large (Table 1), which is often the case in high-end events and indeed is one of the reasons why the high-end storms tend to be more isolated. Large CIN also tends to be related to large CAPE: the synoptic-scale advections and other processes that help stabilize the atmosphere over the lower troposphere, thus leading to CIN, also help destabilize it elsewhere over the troposphere, thus leading to CAPE.

We see in fact from Table 1 that the d03-averaged environmental CAPE in the nine primary PGW experiments is larger than in the CTRL for each event (see also Fig. 4). This is consistent with previous findings on thunderstorm environments under climate change (e.g., Trapp et al. 2007, 2009). Parcel theory has been used to argue that increases in CAPE will result in increases in convective updraft speeds and thus more generally in convective-storm intensity (e.g., Del Genio et al. 2007). Our methodology allows us to quantify to what extent such intensity increases are actually realized.

As evaluated over the d03 area, only four (0510MI, 0510GF, 0510NC, and 0519GF) of the nine primary PGW experiments yielded peaks in convective updraft speeds (w_{peak}) that exceeded the peaks in the relevant CTRL (Fig. 5 and Table 2). If we consider only those three experiments (0510MI, 0510GF, and 0519GF) that generated CTRL-comparable convective storminess over d03, we see that each had a w_{peak} exceeding that in CTRL by more than 15%. How these updraft speeds relate to those predicted by parcel theory and thus CAPE will be considered in section 4.

While insightful, this quantification of convective-updraft speed does not explicitly answer our question about possible changes in the morphology, and therefore in the predominant hazard, of the three events under PGW. We thus consider now the vertical shear of the environmental winds over roughly the lowest half of the troposphere. Besides CAPE, midtropospheric wind shear is the other key environmental control of convective morphology and, implicitly, of intensity. The vertically sheared winds differentially advect precipitation particles out of the updraft and thus promote updraft longevity by reducing the mass loading of the particles. The vertical shear is also a source of horizontal vorticity; in supercell thunderstorms, this is converted into vertical vorticity to become a mesocyclone, which is the parent vortex to tornadoes as well as the structural component that is fundamental to the supercell dynamics (Trapp 2013).

TABLE 1. Quantifications of preconvective/environmental values of CIN, CAPE, S06, and precipitable water (PW), based on d01 (3-km grid length) output but evaluated over the d03 domain for each event and the main experiments. Domain summations are of grid points with the following exceedance thresholds: CIN $\geq 50\,\mathrm{J\,kg^{-1}}$ and $w \geq 2.5\,\mathrm{m\,s^{-1}}$. Based on parcel theory and an experimental adjustment from Crook (1996), the threshold on w equates to the lifting necessary to overcome a CIN of $50\,\mathrm{J\,kg^{-1}}$. The summations are over a 4-h period following CTRL convection initiation within d03 (0000 UTC on 5 May for 0504, 2200 UTC for 0510, and 2100 UTC for 0519). The averages are at the time of the maximum average CAPE in CTRL (0000 UTC on 5 May for 0504 and 0510, 2000 UTC for 0519) within d03.

Event	CMIP5 driver	Expt	$\mathrm{CIN_{avg}}$ ($\mathrm{J\,kg^{-1}}$)	$\sum$CIN	$\sum w\lvert\mathrm{CIN}$	$\mathrm{CAPE_{avg}}$ ($\mathrm{m^2\,s^{-2}}$)	$\mathrm{S06_{avg}}$ ($\mathrm{m\,s^{-1}}$)	$\mathrm{PW_{avg}}$ ($\mathrm{kg\,m^{-2}}$)
0504		CTRL	22	7002	242	3762.6	19.1	26.6
	MIROC5	0504MI	36.5	13928	0	5023.8	16.6	34.5
	GFDL CM3	0504GF	30.1	2694	0	5968.9	21.3	34.0
	CCSM4	0504NC	63	14719	0	4267.2	21.1	28.5
0510		CTRL	81.7	3039	523	1797.3	35.2	40.3
	MIROC5	0510MI	24.3	7472	96	3475	29.7	51.1
	GFDL CM3	0510GF	48.3	7472	827	4012.9	37.1	57.4
	CCSM4	0510NC	61	9656	58	4714.3	30.7	50.8
0519		CTRL	25.1	5170	739	3401.7	21.5	32.8
	MIROC5	0519MI	80.6	11783	30	4381.7	16.9	42.3
	GFDL CM3	0519GF	40.1	4416	656	5175.2	22.7	46.9
	CCSM4	0519NC	44.8	5170	7	5232.5	19.2	41.9

Trapp et al. (2007) found that the magnitude of environmental wind shear evaluated over the 0–6-km layer (S06) tended to decrease in future climates, albeit with geographical and seasonal variations. This shear reduction is in agreement with basic physical arguments—albeit perhaps oversimplified in terms of exact cause and effect (e.g., Grise and Polvani 2014)—that invoke the thermal wind relation and the projection of a decreased pole-to-equator temperature gradient. Taken alone, this could suggest a possible decrease in supercell frequency in favor of an increased frequency for less organized convective storms. Although Diffenbaugh et al. (2013) similarly found an overall decrease in future S06, their analysis indicated that the shear reduction was mostly where and when CAPE was low (i.e., where and when the atmosphere was unsupportive of deep convective storms). Our evaluation of S06 here has its roots in three of the same CMIP5 models used by Diffenbaugh et al. (2013) but is within the context of the PGW modeling methodology. We find that the d03-averaged environmental S06 is lower than CTRL in five of the nine primary PGW experiments but actually higher than CTRL in the remaining four experiments (Table 1). It is noteworthy that three of these four experiments with higher S06 were driven by GFDL CM3 Δs (Table 1).

To help us understand how (or whether) these changes in environmental shear are manifested in terms of morphology and rotational intensity changes, we use calculations of updraft helicity (UH; e.g., see Kain et al. 2008). UH quantifies the degree of spatial correspondence between the convective updraft and storm-generated vertical rotation; high correspondence, and thus high UH, is a supercell hallmark. In weather and climate model applications with grid lengths of 3 to 4 km, UH thresholds of 40–$150\,\mathrm{m^2\,s^2}$ are routinely used to objectively determine supercell existence at model grid points (e.g., Trapp et al. 2011; Clark et al. 2012; Robinson et al. 2013). Because the events herein involve significant tornadic supercells, we used a threshold of $150\,\mathrm{m^2\,s^2}$. Figure 3 indicates that three of the four primary experiments with significant convective storminess (0510MI, 0510GF, and 0519GF) also had UH exceedances within roughly 50% of those in CTRL; these are the same three experiments with a CTRL-exceeding w_{peak} (Fig. 5). We thus claim supercell existence in these experiments; this is consistent with subjective analyses of fields of SRF (not shown), which exhibit characteristic structures such as radar-echo appendages or hooks. Although the fourth primary experiment (0510NC) has only weak supercell justification in terms of exceedances of the (relatively high) UH threshold, it does exhibit these qualitative structures as well. Thus, we classify this experiment as weakly supercellular, with the implication that a change in convective morphology did not occur in any of the PGW experiments with significant convective storminess.

Further calculations of UH and also of vertical vorticity ζ allow for a final quantitative assessment of rotational intensity. Let us consider only those three primary experiments that generated what we have designated as supercells (0510MI, 0510GF, and 0519GF). Two of these three experiments (0510GF and 0519GF) have peaks in UH ($\mathrm{UH_{peak}}$) that exceed their respective CTRL $\mathrm{UH_{peak}}$; both also have peaks in vertical vorticity (ζ_{peak}) that exceed their respective CTRL ζ_{peak}. It is again noteworthy that both of these experiments were driven by GFDL CM3 Δs and had average S06 that exceeded the CTRL S06. Thus, the PGW influence of

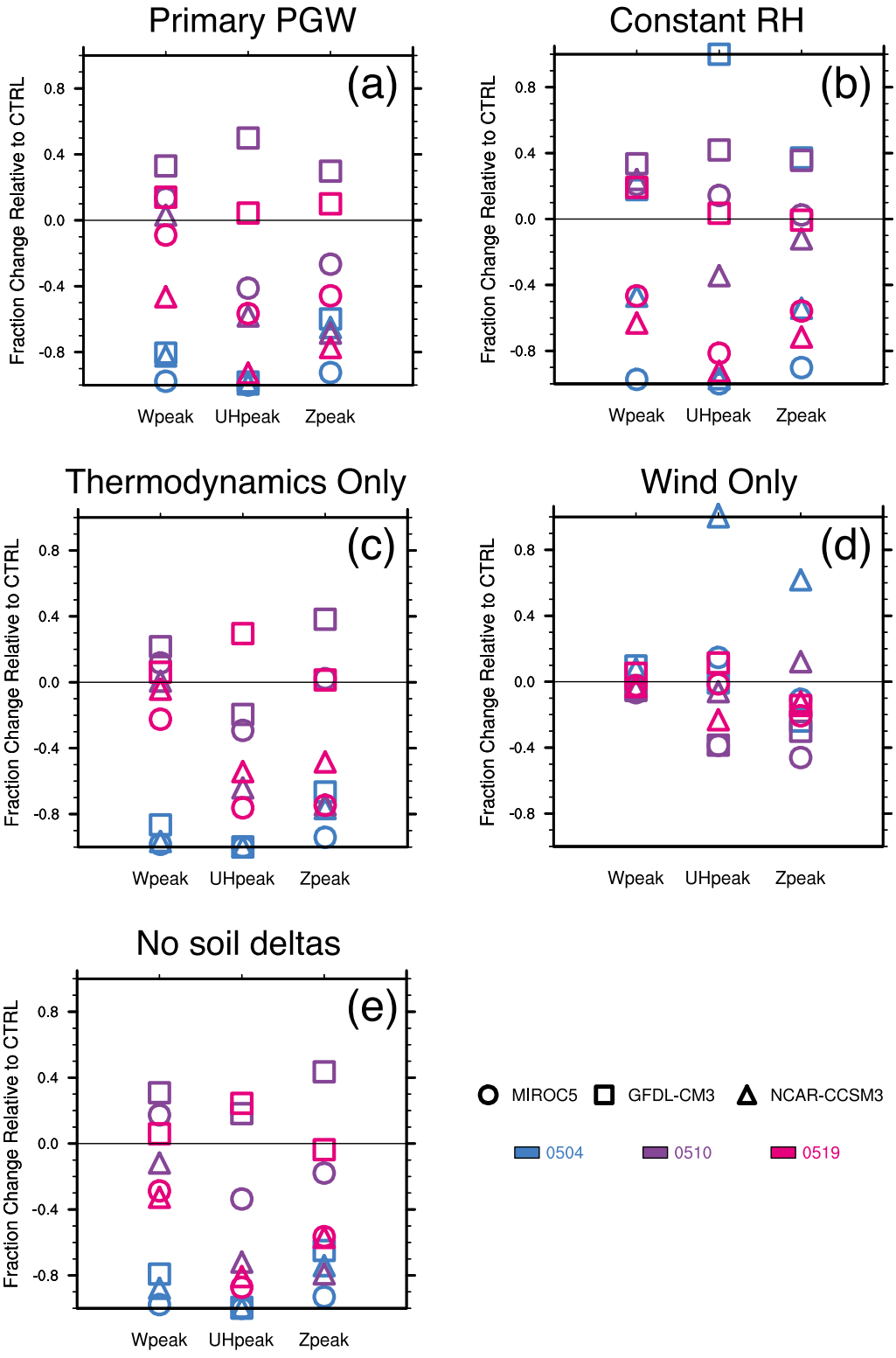

FIG. 5. Peak values of vertical velocity w_{peak}, updraft helicity UH_{peak}, vertical vorticity ζ_{peak}, given as a fractional change relative to CTRL, from (a) primary PGW experiments, (b) constant-RH experiments, (c) experiments with TO climate change Δs, (d) experiments with WO climate change Δs, and (e) experiments with no climate change Δs in soil moisture and temperature. The peaks are evaluated as described in Table 2.

TABLE 2. Storm-scale quantifications of the CTRL experiments, based on d02 (1-km grid length) output but evaluated over the d03 area. The peak values of vertical velocity w_{peak}, updraft helicity UH_{peak}, and vertical vorticity ζ_{peak} are determined over the 4-h period of CTRL storm evolution within d03 (beginning 0130 UTC on 5 May for 0504, 0000 UTC on 11 May for 0510, and 2130 UTC for 0519). Owing to the use of the higher-resolution d02 output, the UH values are much larger here than the thresholds used in Fig. 3.

Event	w_{peak} ($m\,s^{-1}$)	UH_{peak} ($m^2\,s^2$)	ζ_{peak} (s^{-1})	Parcel w_{peak} ($m\,s^{-1}$)
0504	54.58	1244.62	0.0356	86.747
0510	57.75	4271.67	0.1284	59.954
0519	55.56	1349.71	0.043	82.482

GFDL CM3 was one of enhanced CAPE, enhanced S06, and enhanced CIN that was well matched with parcel lifting. Also, the realization of these PGW enhancements was, in both experiments, an intense supercellular storm. The question of whether these more-intense supercells would have generated more-intense tornadoes will be addressed in future work with simulations at higher resolution.

As noted in section 2, additional PGW experiments were conducted to isolate the response from the wind Δs, thermodynamic Δs, and soil moisture and temperature Δs, as well as to examine the effect of a constant-RH assumption. The results of these experiments are event dependent. Figure 5 illustrates that for the 0504 event, all of the experiments with wind-only (WO) Δs yielded supercells with comparable updraft strengths but with a UH_{peak} at or much above that of CTRL. In contrast, all of the experiments with thermodynamic-only (TO) Δs, and without soil (NS) moisture and temperature Δs, failed to initiate convection. Finally, the effects of specific humidity enhancements under the constant-RH experiments only benefited the convective development and intensity driven by the GFDL CM3 Δs.

For the 0510 event, all 12 experiments nominally generated supercells (albeit weakly in the TO and NS experiments; see Figs. 7 and 8). The PGW thermodynamics contributed positively to updraft intensity (w_{peak}) in the experiments with thermodynamic-only Δs and under a constant-RH assumption (Fig. 5). The wind-only Δs generally resulted in a weakening of the rotational characteristics of the supercells. We conclude here that because the baseline (CTRL) wind shear was rather strong in this case, a PGW-modified wind shear was still of sufficient strength to support supercells, and therefore the PGW thermodynamics had the largest overall impact on the rotational intensity.

Finally, Figs. 5–9 show that for the 0519 event, the thermodynamic-only Δs were detrimental to the convective

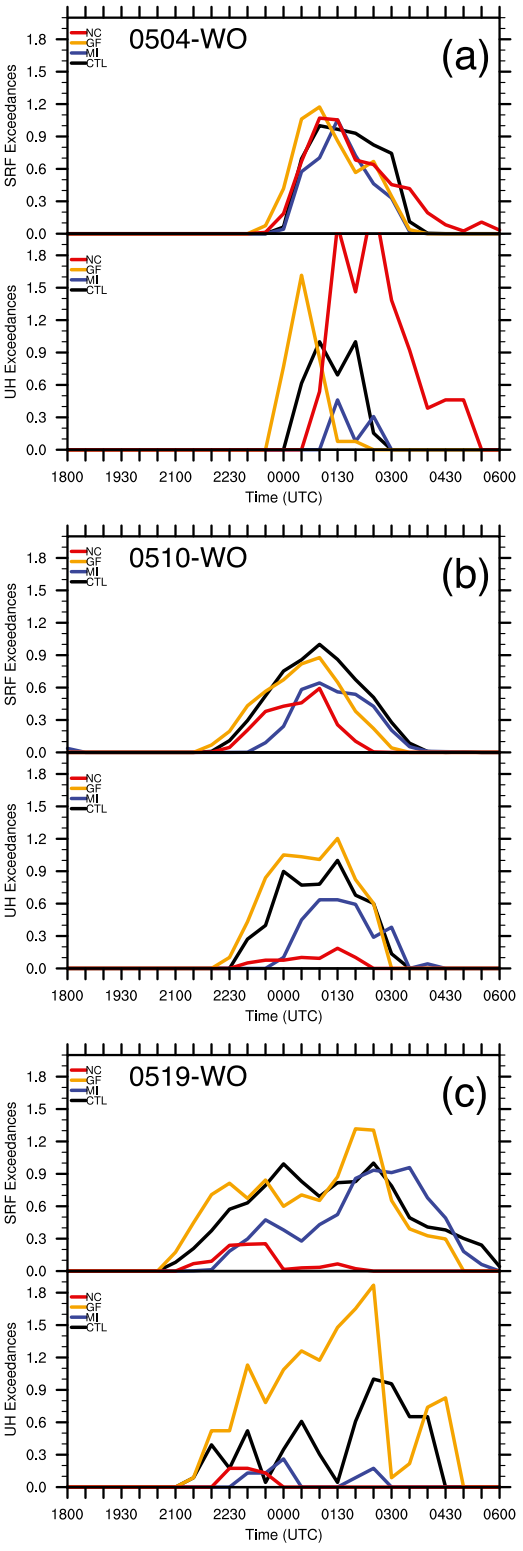

FIG. 6. As in Fig. 3, but for gridpoint exceedances from the WO experiments involving the WO climate change Δs.

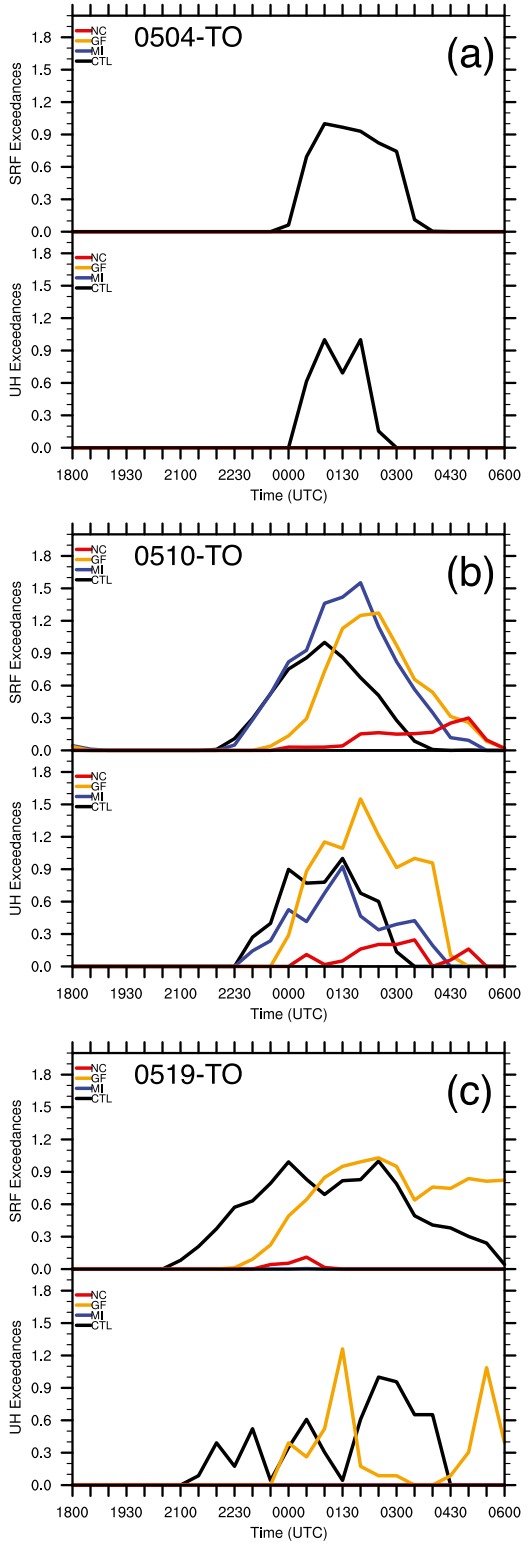

FIG. 7. As in Fig. 3, but for gridpoint exceedances from the TO experiments involving the TO climate change Δs.

development and intensity in the experiments driven by MIROC5 and CCSM4 TO Δs (0519MI-TO and 0519NC-TO) but modestly beneficial to updraft (and rotational) intensity in the GFDL CM3 experiment (0519GF-TO). The experiments with constant-RH and without soil moisture and temperature Δs had similar results. The wind-only Δs allowed for some supercellular organization in each of the experiments, but only as a persistent supercell in 0519GF-WO.

4. Discussion

An important contribution of our application of the PGW methodology is that it provides a means to interpret and perhaps calibrate the results from prior studies using environmental proxies. Indeed, a pervading theme here is the extent to which the preconvective/environmental conditions were converted into a convective intensity and morphology.

Let us first consider CAPE. The parcel theory predictions of peak updraft speeds, which follow from the relationship

$$w_{\text{peak}} = \sqrt{2 \times \text{CAPE}}, \tag{3}$$

are approximately 95–100 m s^{-1} under the PGW represented by the three CMIP5 models used (see Table 1). These are obviously well above the actual speeds diagnosed in the various experiments (Fig. 10). In fact, the ratio of the actual peak to the parcel theory peak is generally less in the PGW experiments than in CTRL, implying less realization of the potential buoyancy under PGW.

One hypothesis for this inequity is that the relatively drier, midtropospheric air under PGW (see Fig. 1) is entrained into the convective updrafts and consequently dilutes their thermal buoyancy. A thorough evaluation of this hypothesis is outside the scope of this current paper, owing to the complexity of directly quantifying entrainment within an evolving field of cumulus clouds (e.g., Dawe and Austin 2012). Another hypothesis—suggested by one of the reviewers—is that the additional precipitable water (PW) under PGW (see Table 1) was converted into more condensate within the updrafts, thus also reducing the updraft buoyancy. This effect is also known as precipitation loading and contributes to the buoyancy term of the vertical equation of motion as $-gq_T$, where g is gravity and q_T is the total condensate (rain, graupel/hail, snow, cloud water, and cloud ice) mixing ratio. It was most straightforward for us to quantify the amount of condensate in updraft cores, at heights where precipitation generation and growth in rising air was expected. Figure 11 indicates that, for

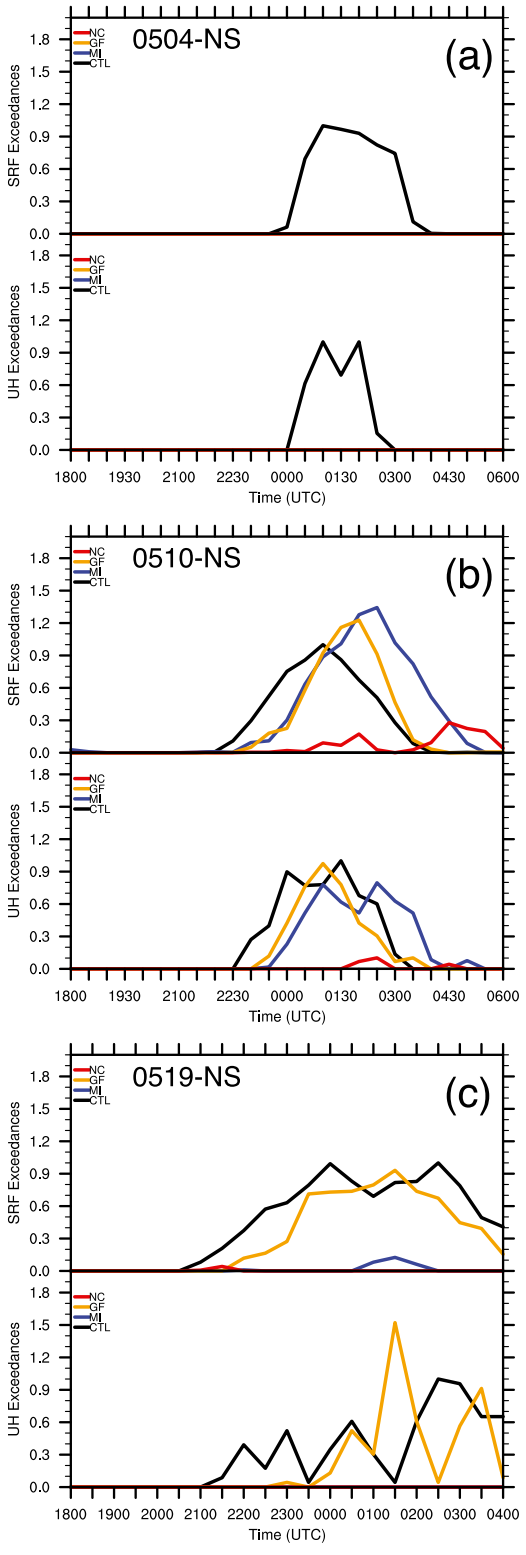

FIG. 8. As in Fig. 3, but for gridpoint exceedances from the NS experiments that exclude the soil moisture and temperature climate change Δs.

example, the amount of graupel is larger within moderately strong updrafts under PGW than within the corresponding CTRL updrafts. A similar conclusion was reached with quantifications at different heights and for the different condensate species. Thus, Fig. 11 appears to support this hypothesis, providing a physical cause for the finding that the updrafts are more intense under PGW but not in proportion to the projected higher levels of CAPE.

The dependence of rotational intensity on the magnitude of the environmental vertical wind shear is not as straightforward as Eq. (3) but can be partly expressed using a simplified, linearized form of the vertical vorticity equation:

$$\zeta \sim (w/c) \times \mathrm{S06}, \tag{4}$$

which assumes, for the purpose of argument only, that S06 comprises the vertical shear of the environmental zonal wind only, and c is considered a coefficient of proportionality, even though strictly it encompasses the speed of the storm (e.g., see Trapp 2013). Despite the simplifications of Eq. (4), Tables 1 and 2 and Fig. 5 reveal that the largest ζ_{peak} (and $\mathrm{UH}_{\mathrm{peak}}$) values are indeed found in the cases with the largest w_{peak} and highest S06. We conclude the scaling between ζ_{peak}, w_{peak}, and S06 embodied in Eq. (4) appears to apply in the same way to PGW storms as to storms from CTRL and thus, unlike the scaling between w_{peak} and CAPE, appears to be insensitive to PGW.

It is unclear whether a similar comment can be made regarding the expected morphology versus actual morphology because the dependence of convective morphology on the combined influences of S06 and CAPE is mostly empirical (e.g., Weisman and Klemp 1982). To put the actual morphology in the context of the environmental proxy-based studies, the product S06 × CAPE in each of our experiments (including CTRL) is several times the 10 000 or even 20 000 threshold used to identify a potential severe-thunderstorm environment (e.g., Trapp et al. 2007; Brooks 2013; Diffenbaugh et al. 2013). It is important to note that the "severe thunderstorm" is not in itself a separate morphology. Moreover, there is no explicit relationship between this environmental threshold and morphology, even though the implicit expectation is that many of the severe hail, wind, and tornado-bearing storms would indeed be supercells (e.g., Duda and Gallus 2010). Especially in light of the inflated CAPE values [relative to w_{peak} via Eq. (3)], a higher threshold on S06 × CAPE would seem appropriate when environmental proxies of high-end tornadic supercells are desired.

Finally, thresholds of CIN would not have been particularly successful here in predicting the environments

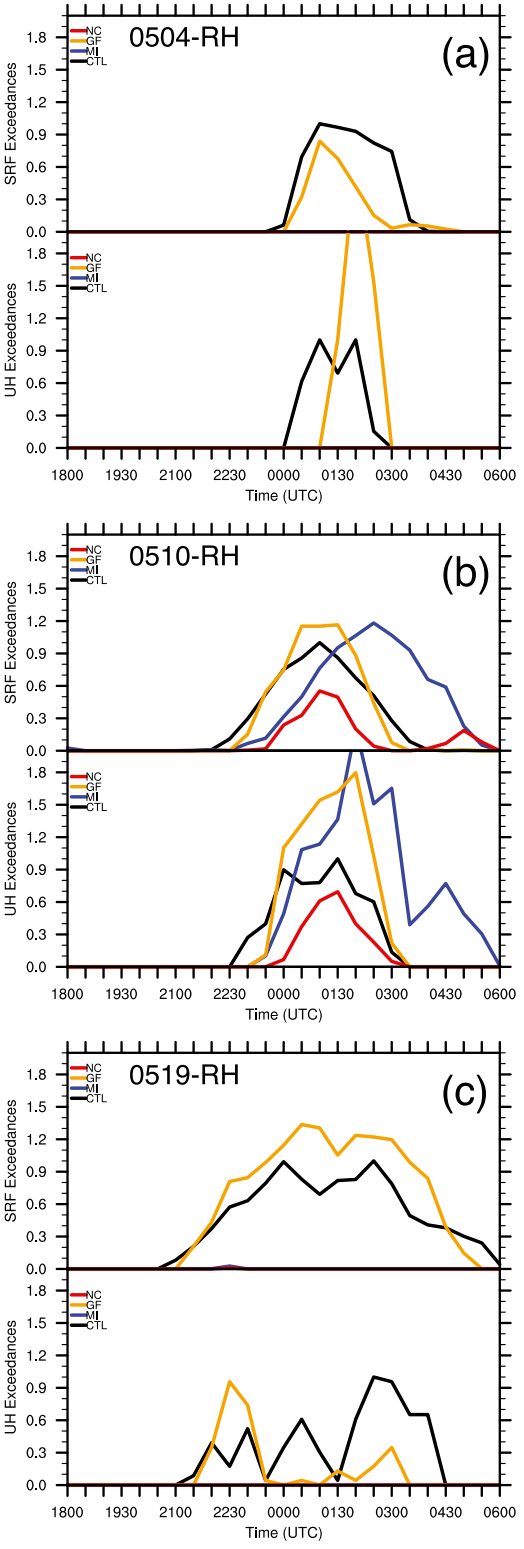

FIG. 9. As in Fig. 3, but for gridpoint exceedances from the RH experiments with a constant-RH assumption (and thus which exclude the RH climate change Δs).

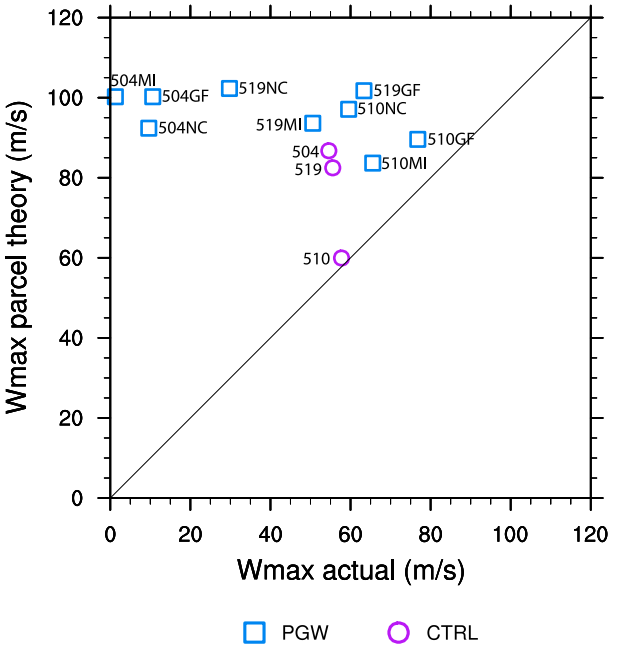

FIG. 10. Scatterplot of peak values of vertical velocity ($m\,s^{-1}$) vs peak values predicted by parcel theory ($m\,s^{-1}$) using the maximum preconvective average CAPE (see Table 1).

that allowed the initiation of supercellular convection. Indeed, not until we combined CIN locally with a quantification of the preconvective/environmental vertical motions were we able to explain why some experiments generated convective storms and others did not. This issue of convection initiation will continue to vex GCM-based environmental proxy approaches, arguing for the continued development and application of high-resolution dynamical downscaling approaches.

5. Summary and conclusions

The objective of this research was to answer the basic question of how current-day tornadic-supercellular storm events might be realized under future anthropogenic climate change. We adapted the pseudo global warming (PGW) methodology as employed by Lackmann (2013, 2015) and used three contributions to the CMIP5 archive to obtain the mean 3D atmospheric state simulated during May 1990–99 and May 2090–99. The differences, or climate change Δs, in temperature, relative humidity, pressure, and winds were added to NWP analyses (NAM-ANL) of three high-end tornadic storm events, and this modified atmospheric state was then used for initial and boundary conditions for real-data WRF Model simulations of the events at high resolution. Comparison of an ensemble of these simulations with control simulations (CTRL) facilitated assessment of PGW effects.

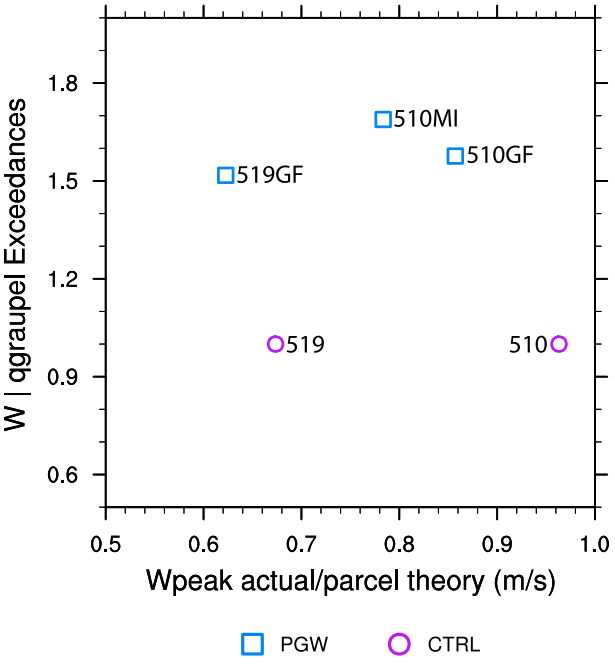

FIG. 11. Scatterplot of normalized peak values of vertical velocity vs the number of exceedances of graupel mixing ratio ($q_g > 0.005\,\mathrm{kg\,kg^{-1}}$ at $z = 5$ km) conditioned on the coexistence of $w > 25\,\mathrm{m\,s^{-1}}$ at $z = 5$ km. Only the experiments that had supercellular convection under PGW were considered.

In contrast to the robust development of supercellular convection in each CTRL, the combined effects of increased CIN and decreased parcel lifting under PGW led to a failure of convection initiation in many of the ensemble members. Those members that had sufficient matching between the CIN and lifting tended to generate stronger convective updrafts than CTRL because of the relatively higher CAPE under PGW. In addition, the members with enhanced updrafts also tended to have enhanced vertical rotation. In fact, such mesocyclonic rotation and attendant supercellular morphology were even found in simulations that were driven with PGW-reduced environmental wind shear. Notably, the PGW modifications did not induce a change in the convective morphology in any of the PGW experiments with significant convective storminess.

Our application of the PGW methodology also provided some additional insight into, and perhaps some alternative interpretations of, the results from prior studies that used environmental proxies. We found, for example, that the updrafts simulated under PGW were more relatively intense, but not in proportion to the projected higher levels of CAPE. As estimated by the amount of graupel in updraft cores, we found that the effects of precipitation loading and its associated reduction of updraft buoyancy were higher in PGW updrafts. The basic conclusion here is that projected extreme values of CAPE have the potential to lead to convective updrafts that are strong, but not necessarily extremely strong.

These conclusions are of course limited by the number of events and set of different climate change Δs. Accordingly, our forthcoming work will incorporate a larger set of climate change Δs and consider how relatively more benign convective storm events, and other morphologies, are realized under PGW. It will use higher-resolution grids to allow consideration of tornado intensity. Finally, it will reveal how current-day convective-storm events might evolve within a historical (i.e., late nineteenth century) environment, thus providing us with a possible framework for attribution studies.

Acknowledgments. We acknowledge the World Climate Research Programme's Working Group on Coupled Modelling, which is responsible for CMIP, and thank the MIROC, GFDL, and NCAR climate modeling groups for producing and making available their model output. We also acknowledge the two anonymous reviewers for providing helpful comments.

REFERENCES

Brooks, H. E., 2013: Severe thunderstorms and climate change. *Atmos. Res.*, **123**, 129–138, doi:10.1016/j.atmosres.2012.04.002.

——, and C. A. Doswell III, 2001: Some aspects of the international climatology of tornadoes by damage classification. *Atmos. Res.*, **56**, 191–201, doi:10.1016/S0169-8095(00)00098-3.

——, C. A. Doswell, and M. P. Kay, 2003a: Climatological estimates of local daily tornado probability for the United States. *Wea. Forecasting*, **18**, 626–640, doi:10.1175/1520-0434(2003)018<0626:CEOLDT>2.0.CO;2.

——, J. W. Lee, and J. P. Craven, 2003b: The spatial distribution of severe thunderstorm and tornado environments from global reanalysis data. *Atmos. Res.*, **67–68**, 73–94, doi:10.1016/S0169-8095(03)00045-0.

Chen, F., and J. Dudhia, 2001: Coupling an advanced land surface–hydrology model with the Penn State–NCAR MM5 modeling system. Part I: Model implementation and sensitivity. *Mon. Wea. Rev.*, **129**, 569–585, doi:10.1175/1520-0493(2001)129<0569:CAALSH>2.0.CO;2.

Chou, M. D., and M. J. Suarez, 1999: A solar radiation parameterization for atmospheric studies. NASA Tech. Rep. NASA/TM-1999-10460, 38 pp.

Clark, A. J., J. S. Kain, P. T. Marsh, J. Correia, M. Xue, and F. Kong, 2012: Forecasting tornado pathlengths using a three-dimensional object identification algorithm applied to convection-allowing forecasts. *Wea. Forecasting*, **27**, 1090–1113, doi:10.1175/WAF-D-11-00147.1.

Crook, N. A., 1996: Sensitivity of moist convection forced by boundary layer processes to low-level thermodynamic fields. *Mon. Wea. Rev.*, **124**, 1767–1785, doi:10.1175/1520-0493(1996)124<1767:SOMCFB>2.0.CO;2.

Dawe, J. T., and P. H. Austin, 2012: Statistical analysis of an LES shallow cumulus cloud ensemble using a cloud tracking algorithm. *Atmos. Chem. Phys.*, **12**, 1101–1119, doi:10.5194/acp-12-1101-2012.

Del Genio, A. D., M.-S. Yao, and J. Jonas, 2007: Will moist convection be stronger in a warmer climate? *Geophys. Res. Lett.*, **34**, L16703, doi:10.1029/2007GL030525.

Diffenbaugh, N. S., M. Scherer, and R. J. Trapp, 2013: Robust increases in severe thunderstorm environments in response to greenhouse forcing. *Proc. Natl. Acad. Sci. USA*, **110**, 16 361–16 366, doi:10.1073/pnas.1307758110.

Duda, J. D., and W. A. Gallus, 2010: Spring and summer midwestern severe weather reports in supercells compared to other morphologies. *Wea. Forecasting*, **25**, 190–206, doi:10.1175/2009WAF2222338.1.

Frei, C., C. Schär, D. Lüthi, and H. C. Davies, 1998: Heavy precipitation processes in a warmer climate. *Geophys. Res. Lett.*, **25**, 1431–1434, doi:10.1029/98GL51099.

Gensini, V. A., and T. L. Mote, 2014: Estimations of hazardous convective weather in the United States using dynamical downscaling. *J. Climate*, **27**, 6581–6589, doi:10.1175/JCLI-D-13-00777.1.

——, and ——, 2015: Downscaled estimates of late 21st century severe weather from CCSM3. *Climatic Change*, **129**, 307–321, doi:10.1007/s10584-014-1320-z.

Grams, J. S., R. L. Thompson, D. V. Snively, J. A. Prentice, G. M. Hodges, and L. J. Reames, 2012: A climatology and comparison of parameters for significant tornado events in the United States. *Wea. Forecasting*, **27**, 106–123, doi:10.1175/WAF-D-11-00008.1.

Grise, K. M., and L. M. Polvani, 2014: The response of midlatitude jets to increased CO_2: Distinguishing the roles of sea surface temperature and direct radiative forcing. *Geophys. Res. Lett.*, **41**, 6863–6871, doi:10.1002/2014GL061638.

Janjić, Z. I., 1994: The step-mountain eta coordinate model: Further developments of the convection, viscous sublayer, and turbulence closure schemes. *Mon. Wea. Rev.*, **122**, 927–945, doi:10.1175/1520-0493(1994)122<0927:TSMECM>2.0.CO;2.

Kain, J. S., and Coauthors, 2008: Some practical considerations regarding horizontal resolution in the first generation of operational convection-allowing NWP. *Wea. Forecasting*, **23**, 931–952, doi:10.1175/WAF2007106.1.

Lackmann, G. M., 2013: The south-central U.S. flood of May 2010: Present and future. *J. Climate*, **26**, 4688–4709, doi:10.1175/JCLI-D-12-00392.1.

——, 2015: Hurricane Sandy before 1900 and after 2100. *Bull. Amer. Meteor. Soc.*, **96**, 547–560, doi:10.1175/BAMS-D-14-00123.1.

Marsh, P. T., H. E. Brooks, and D. J. Karoly, 2007: Assessment of the severe weather environment in North America simulated by a global climate model. *Atmos. Sci. Lett.*, **8**, 100–106, doi:10.1002/asl.159.

Morrison, H., G. Thompson, and V. Tatarskii, 2009: Impact of cloud microphysics on the development of trailing stratiform precipitation in a simulated squall line: Comparison of one- and two-moment schemes. *Mon. Wea. Rev.*, **137**, 991–1007, doi:10.1175/2008MWR2556.1.

Rasmussen, R., and Coauthors, 2011: High-resolution coupled climate runoff simulations of seasonal snowfall over Colorado: A process study of current and warmer climate. *J. Climate*, **24**, 3015–3048, doi:10.1175/2010JCLI3985.1.

Robinson, E. D., R. J. Trapp, and M. E. Baldwin, 2013: The geospatial and temporal distributions of severe thunderstorms from high-resolution dynamical downscaling. *J. Appl. Meteor. Climatol.*, **52**, 2147–2161, doi:10.1175/JAMC-D-12-0131.1.

Schär, C., C. Frei, D. Lüthi, and H. C. Davies, 1996: Surrogate climate-change scenarios for regional climate models. *Geophys. Res. Lett.*, **23**, 669–672, doi:10.1029/96GL00265.

Skamarock, W. C., 2004: Evaluating mesoscale NWP models using kinetic energy spectra. *Mon. Wea. Rev.*, **132**, 3019–3032, doi:10.1175/MWR2830.1.

——, J. B. Klemp, J. Dudhia, D. O. Gill, D. M. Barker, X.-Y. Huang, W. Wang, and J. G. Powers, 2008: A description of the Advanced Research WRF version 3. NCAR Tech. Note NCAR/TN-475+STR, 113 pp. [Available online at http://www2.mmm.ucar.edu/wrf/users/docs/arw_v3.pdf.]

Thompson, R. L., B. T. Smith, J. S. Grams, A. R. Dean, and C. Broyles, 2012: Convective modes for significant severe thunderstorms in the contiguous United States. Part II: Supercell and QLCS tornado environments. *Wea. Forecasting*, **27**, 1136–1154, doi:10.1175/WAF-D-11-00116.1.

Trapp, R. J., 2013: *Mesoscale-Convective Processes in the Atmosphere.* Cambridge University Press, 346 pp.

——, S. A. Tessendorf, E. S. Godfrey, and H. E. Brooks, 2005: Tornadoes from squall lines and bow echoes. Part I: Climatological distribution. *Wea. Forecasting*, **20**, 23–34, doi:10.1175/WAF-835.1.

——, N. S. Diffenbaugh, H. E. Brooks, M. E. Baldwin, E. D. Robinson, and J. S. Pal, 2007: Changes in severe thunderstorm environment frequency during the 21st century caused by anthropogenically enhanced global radiative forcing. *Proc. Natl. Acad. Sci. USA*, **104**, 19 719–19 723, doi:10.1073/pnas.0705494104.

——, ——, and A. Gluhovsky, 2009: Transient response of severe thunderstorm forcing to elevated greenhouse gas concentrations. *Geophys. Res. Lett.*, **36**, L01703, doi:10.1029/2008GL036203.

——, E. Robinson, M. Baldwin, N. Diffenbaugh, and B. J. Schwedler, 2011: Regional climate of hazardous convective weather through high-resolution dynamical downscaling. *Climate Dyn.*, **37**, 677–688, doi:10.1007/s00382-010-0826-y.

Van Leer, K., 2013: Storm mergers and their role in tornado genesis during the 2011 Joplin storm. M.S. thesis, Dept. of Atmospheric Sciences, University of Illinois at Urbana–Champaign, 82 pp.

Weisman, M. L., and J. B. Klemp, 1982: The dependence of numerically simulated convective storms on vertical wind shear and buoyancy. *Mon. Wea. Rev.*, **110**, 504–520, doi:10.1175/1520-0493(1982)110<0504:TDONSC>2.0.CO;2.